# Supporting Information

## Efficient selective hydrogenation of phenylacetylene over intermetallic Ni-Sb catalyst

Yao Fan,[a] Chenyang Lu,[*a] Aonan Zeng,[b] Yinjie Deng,[c] Ling Qin,[c] Shihong Zhou,[a] Mengxin Wang,[a] Anjie Wang,[b] Luxi Tan,[*a] Lichun Dong[*a]

## Experimental Section

### Preparation of $Ni/SiO_2$ and $Ni_xSb_y/SiO_2$

Firstly, stoichiometric $NiCl_2$ and/or $SbCl_3$ were dissolved in the hydrochloric acid solution to make a mixed salt solution. The resulting mixture was added dropwise into the $SiO_2$ support under continuous stirring, followed by aging for 24 hours to afford the chloride precursor. The precursor was then reduced at 800 ℃ in $H_2$ for 1 h. After cooling to room temperature, the resulting product was ground into a fine powder using an agate mortar, yielding $SiO_2$-supported $Ni_xSb_y$ intermetallic compounds and monometallic Ni catalysts.

### Preparation of $Sb/SiO_2$ and $Sb/SiO_2$-H

An appropriate amount of antimony powder was thoroughly mixed with $SiO_2$ powder. The mixture was then placed into a ball-milling jar with agate beads of varying sizes, followed by mechanical ball milling at 600 rpm for 1 h, denoted as $Sb/SiO_2$. Then the $Sb/SiO_2$ sample by mixing Sb and $SiO_2$ was treated in $H_2$ at 800 ℃ for 1 h, which is following the same method for preparing $Ni_xSb_y/SiO_2$ (denoted as $Sb/SiO_2$-H).

### Characterization

The powder X-ray diffraction (XRD) measurement was conducted on a PANalytical X-ray diffractometer with Cu Kα radiation (40 kV, 100 mA). The scanning ranged from 10° to 80° with a scanning speed of 8 °/min. Transmission electron microscopy (TEM), high-resolution transmission electron microscopy (HRTEM) and energy-dispersive X-ray spectroscopy (EDS) elemental mapping images were obtained on a Talos F200S microscope. X-ray photoelectron spectroscopy (XPS) measurement was performed on a Scientific K-Alpha spectrometer equipped with a monochromatic Al Kα excitation source (hν = 1486.6 eV). All binding energies were calibrated with reference to the C 1 s peak (284.8 eV). Ni contents in different materials were quantified using inductively coupled plasma optical emission spectrometry (ICP-AES, Agilent 5110). Hydrogen temperature-programmed desorption ($H_2$-TPD) measurements were conducted using a GC (FULI 9790II) analyzer with a thermal conductivity detector (TCD). In a typical process, the sample (50 mg) was loaded into a U-shaped quartz tube, pretreated under a $H_2$ and Ar mixture (1:9, v/v) at 400 ℃ for 1 h. Subsequently, the reduced sample was

purged in Ar at 400 ℃ for 30 min, then cooled down to room temperatur. After $H_2$ adsorption saturation, the system was flushed with Ar for 30 min. Finally, the temperature was increased to 500 ℃ at a heating rate of 10 ℃ $min^{-1}$ under Ar flow, and the desorption profiles were recorded. Nitrogen adsorption-desorption isotherms were measured at -196 ℃ on a Micromeritics Tristar II 3020 instrument. The specific surface area was calculated according to the Brumauer–Emmett–Teller method, while the pore volume and average pore size were calculated from the desorption branch of the $N_2$ adsorption–desorption isotherm by the Barrett–Joyner–Halenda method.

**Catalytic Performance**

Semi-hydrogenation of phenylacetylene was conducted in a 100 mL micro mechanical stirred reactor. Initially, ethanol (20 mL), phenylacetylene (2 mmol), and the catalyst (100 mg) were loaded into the reactor. Subsequently, purge with $H_2$ ten times to remove air from the reactor. The reaction proceeded under 2 MPa $H_2$ pressure with programmed temperature control and stirring at 200 rpm for 2 h. The liquid-phase composition was analyzed offline using gas chromatography (Nexis GC-2030) to track changes with temperature. The phenylacetylene conversion and product selectivity were calculated as follows.

$$C_8H_6 \text{ conversion} = \frac{c_0 - c_0'}{c_0} \times 100\% \quad (1)$$

$$C_8H_8 \text{ selectivity} = \frac{c_1}{c_1 + c_2} \times 100\% \quad (2)$$

$$C_8H_{10} \text{ selectivity} = \frac{c_2}{c_1 + c_2} \times 100\% \quad (3)$$

where $c_0$ and $c_0'$ represent the concentrations of phenylacetylene before and after the reaction, respectively, while $c_1$ and $c_2$ denote the concentrations of styrene and ethylbenzene in the product, respectively.

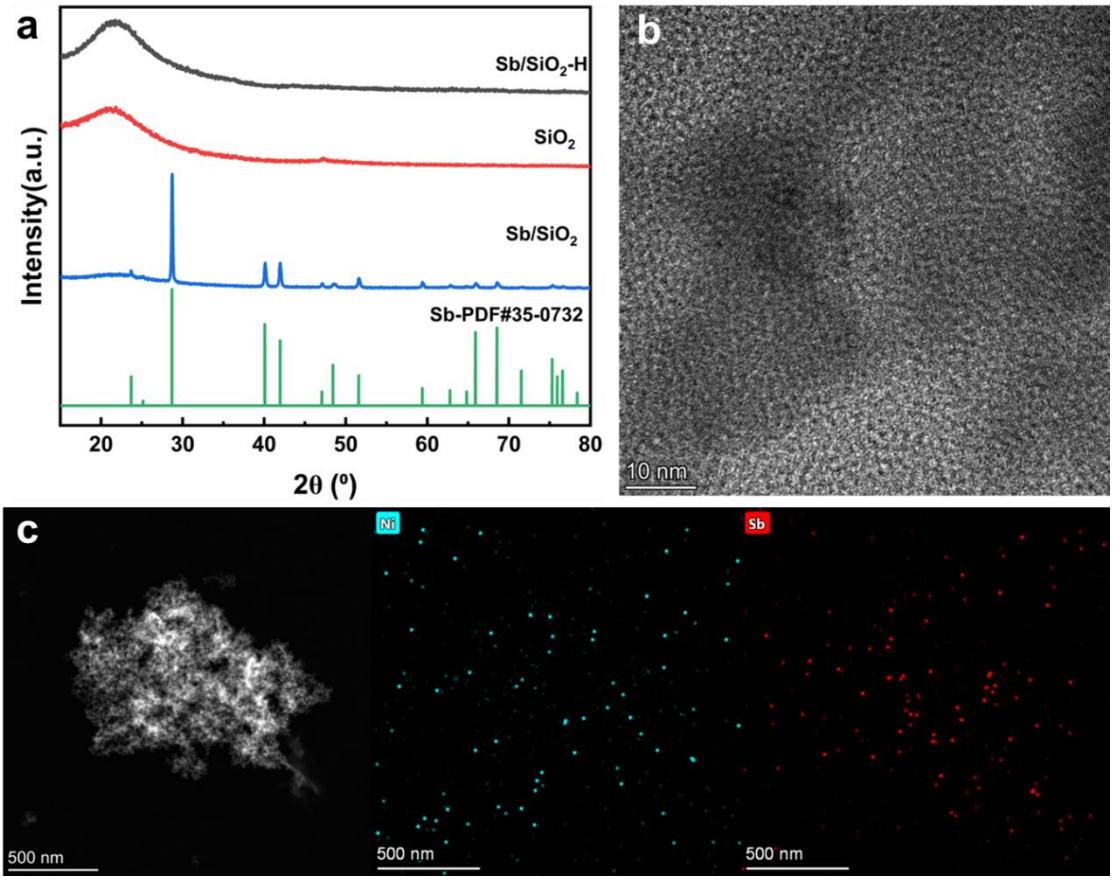


**Fig. S1** (a) XRD pattern, (b) HRTEM and (c) EDS-mapping images of $Sb/SiO_2$-H.

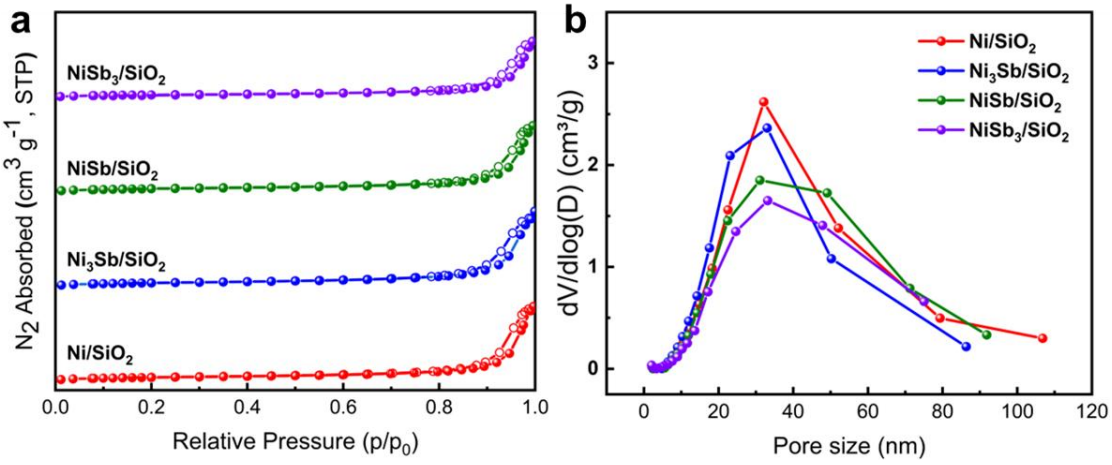


**Fig. S2** (a) $N_2$ adsorption-desorption isotherms and (b) pore size distribution of the $Ni_xSb_y/SiO_2$ catalysts.

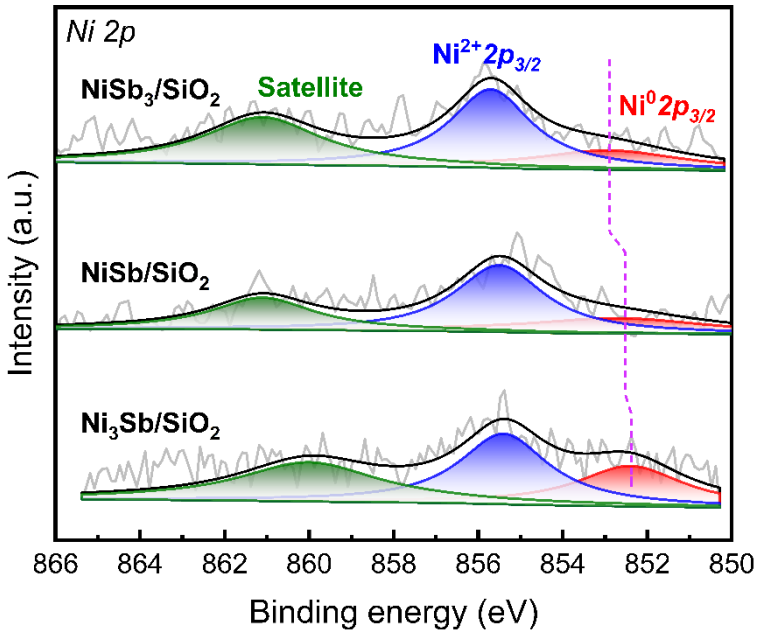


**Fig. S3** Ni 2p XPS spectra of the $NiSb_3/SiO_2$, $NiSb/SiO_2$ and $Ni_3Sb/SiO_2$ catalysts.

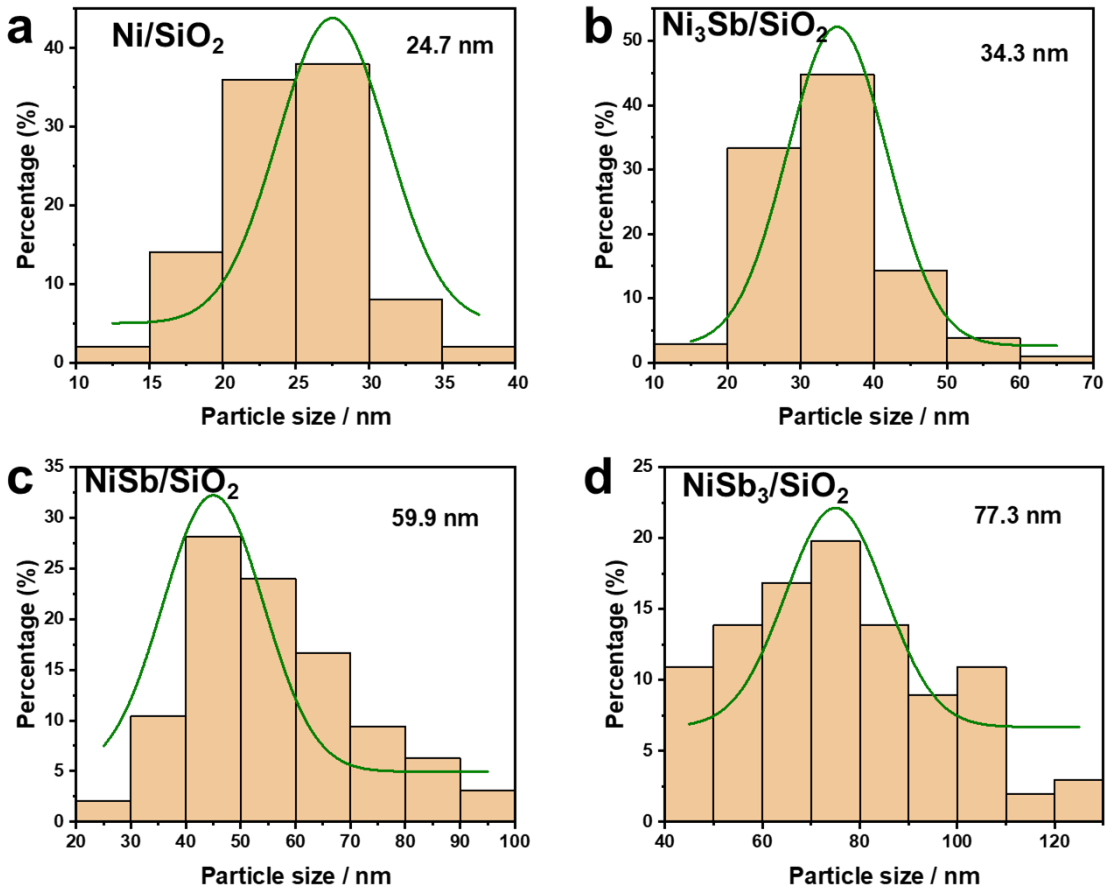


**Fig. S4.** Particle size distribution of (a) $Ni/SiO_2$, (b) $Ni_3Sb/SiO_2$, (c) $NiSb/SiO_2$ and (d) $NiSb_3/SiO_2$.

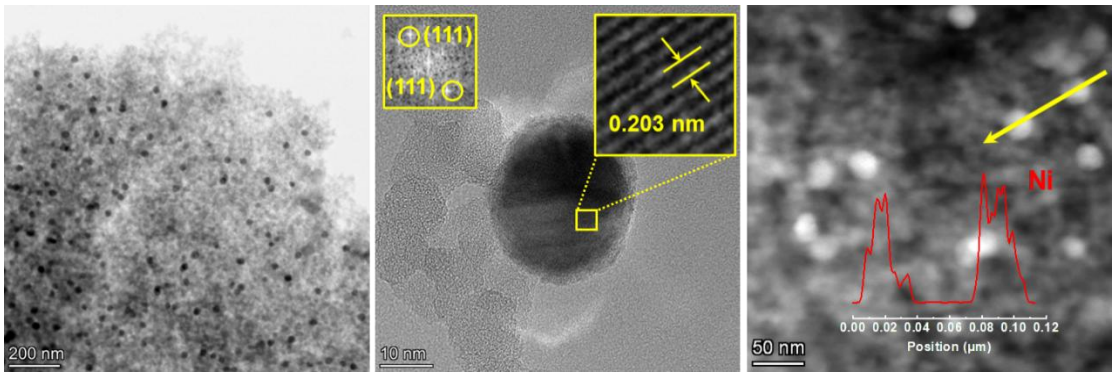


**Fig. S5** HRTEM images, associated FFT pattern and EDS line-scanning profile for the $Ni/SiO_2$ catalyst.

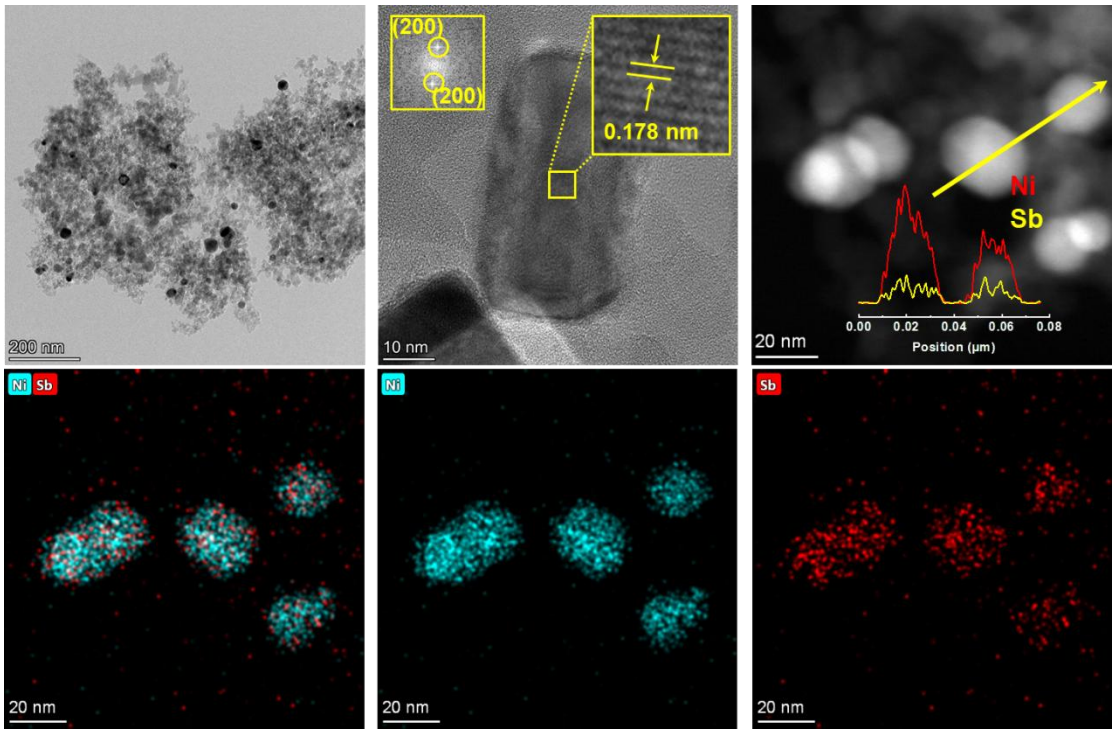


**Fig. S6** HRTEM images, associated FFT pattern, EDS mapping images and line-scanning profile for the $Ni_3Sb/SiO_2$ catalyst.

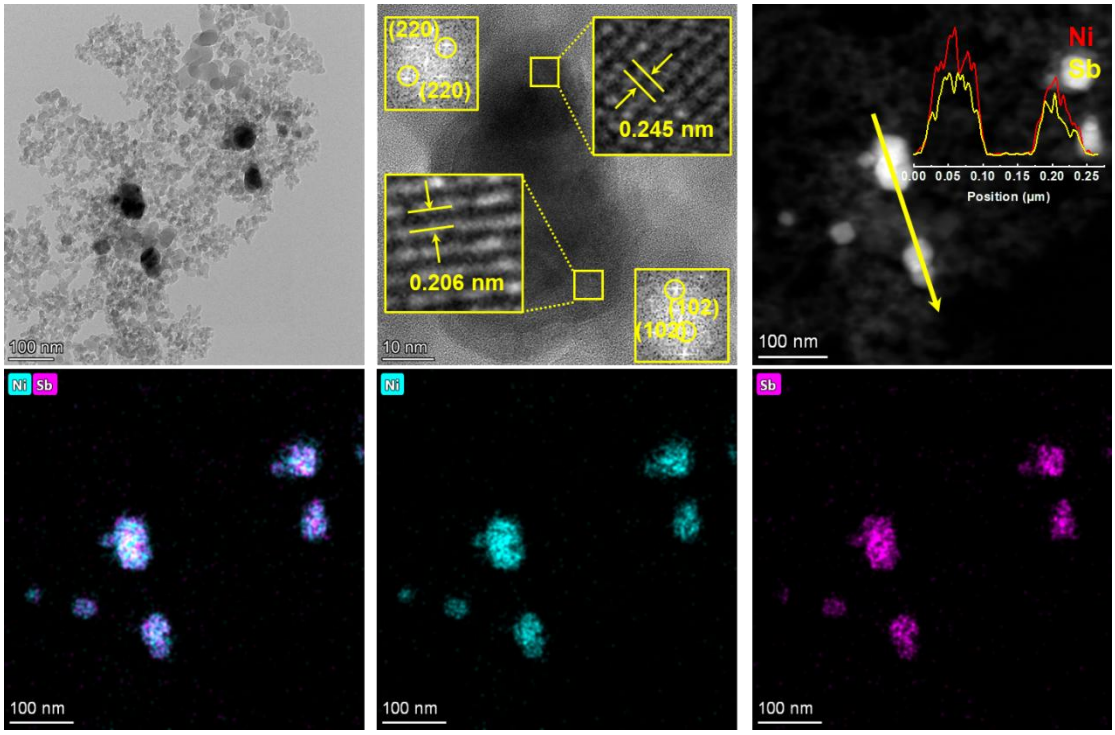


**Fig. S7** HRTEM images, associated FFT pattern, EDS mapping images and line-scanning profile for the $NiSb/SiO_2$ catalyst.

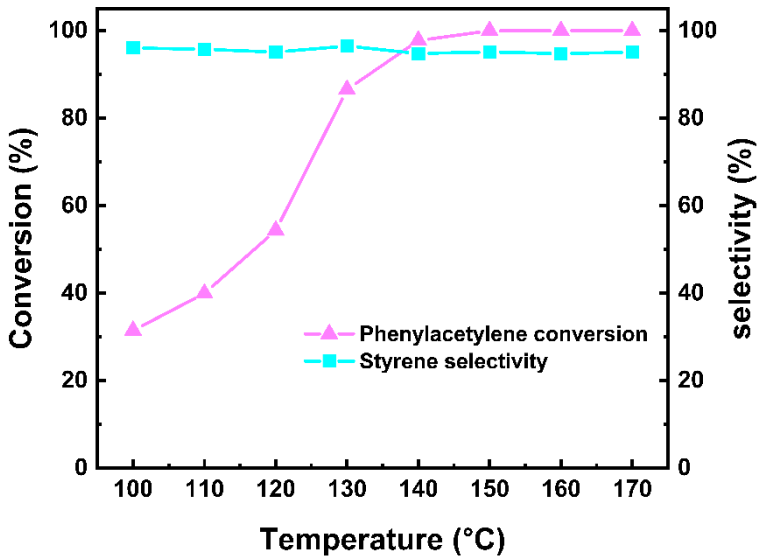


**Fig. S8** Phenylacetylene conversion and styrene selectivity as a function of reaction temperature over $NiSb_3/SiO_2$.

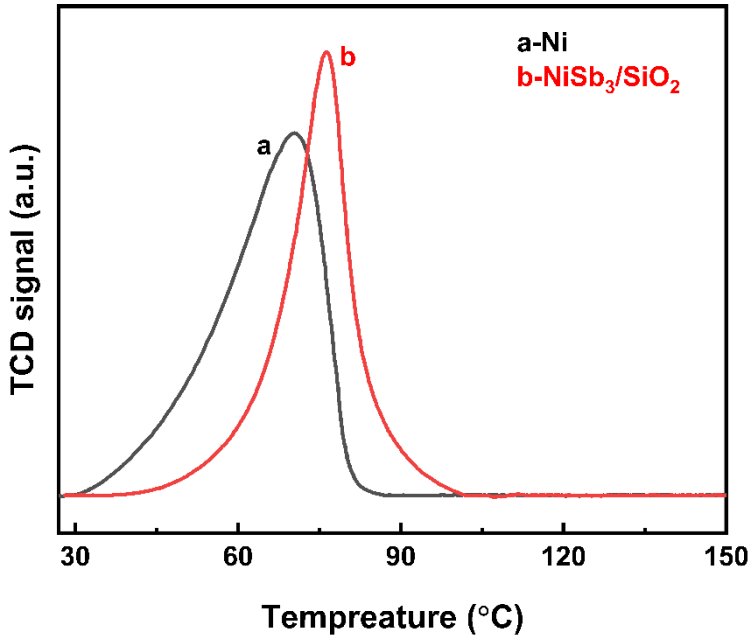


**Fig. S9** $H_2$-TPD profiles of $Ni/SiO_2$ and $NiSb_3/SiO_2$.

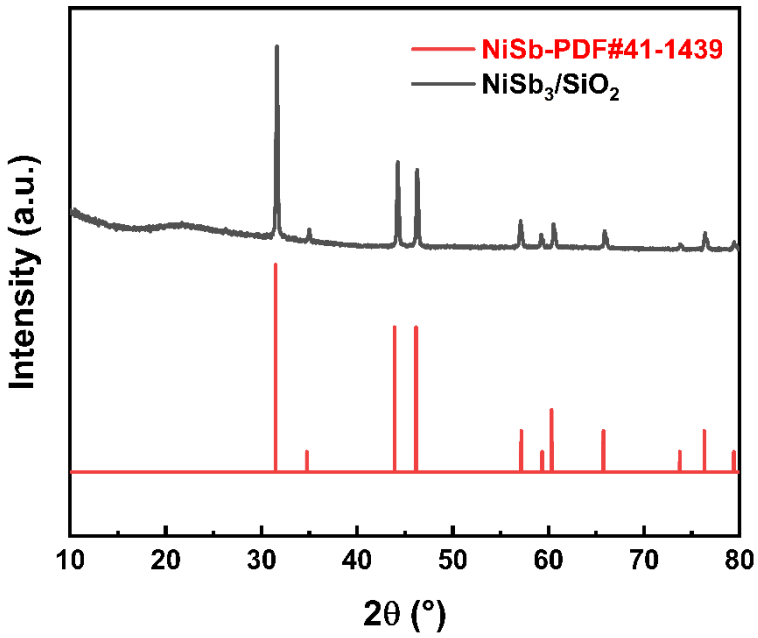


**Fig. S10** XRD pattern of the spent $NiSb_3/SiO_2$ catalyst after ten reactions.

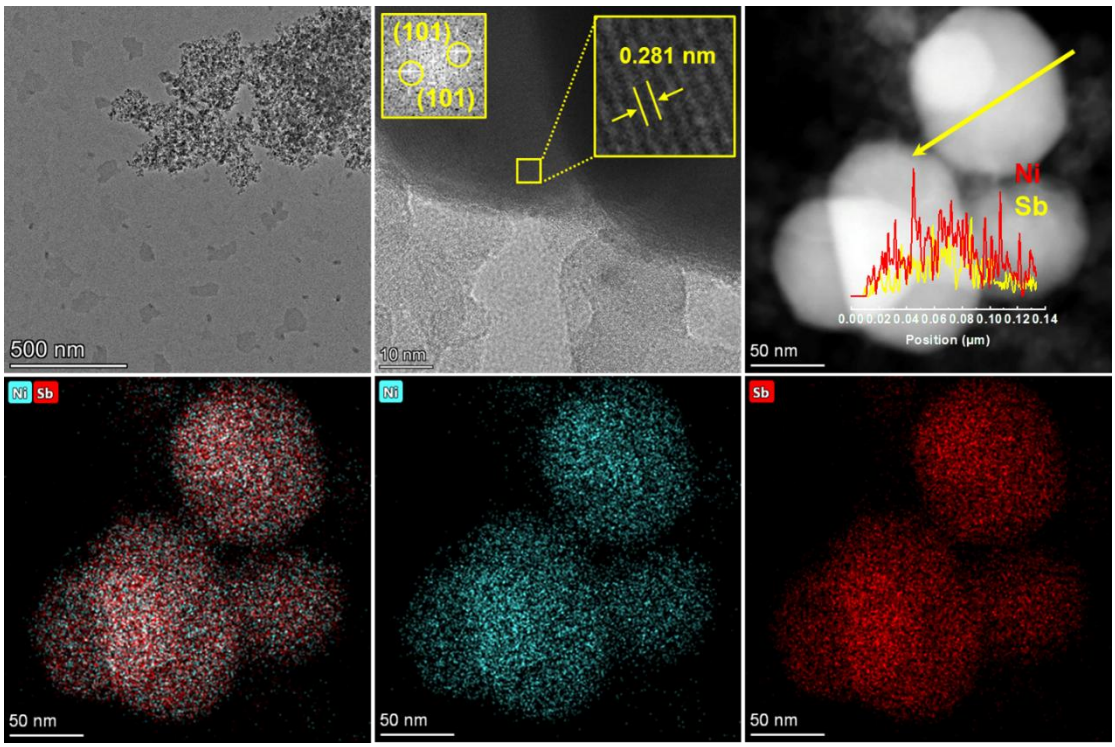


**Fig. S11** HRTEM images, associated FFT pattern, EDS mapping images and line-scanning profile for the spent $NiSb_3/SiO_2$ catalyst.

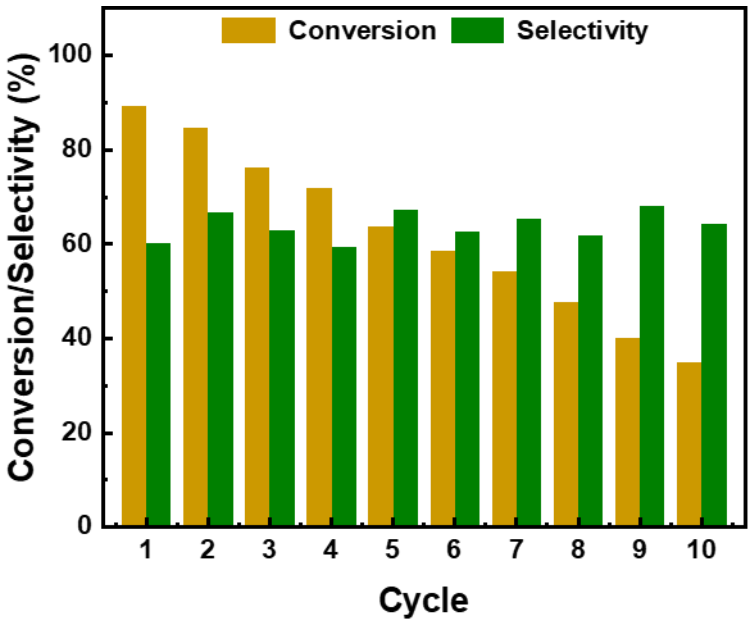


**Fig. S12** Stability test of $Ni/SiO_2$.

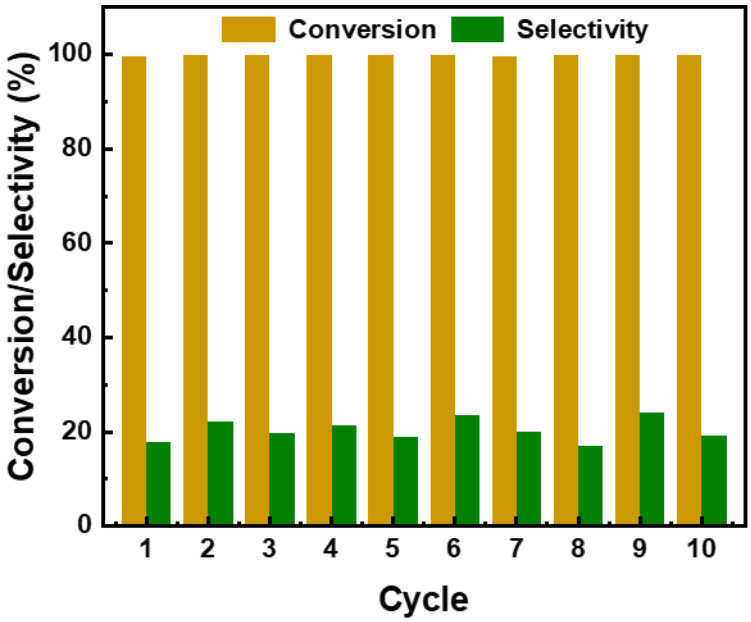


**Fig. S13** Stability test of $Ni_3Sb/SiO_2$.

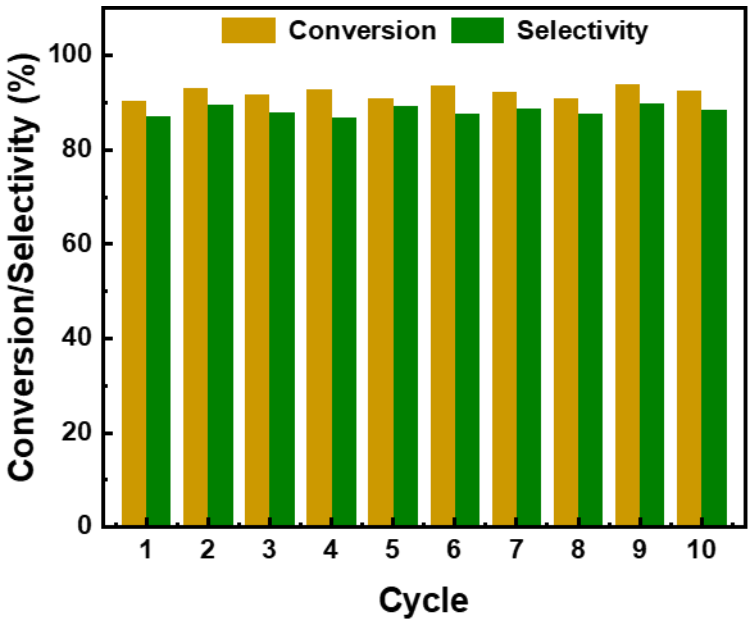


**Fig. S14** Stability test of $NiSb/SiO_2$.

**Table S1** The Ni loading of the supported Ni-based catalysts determined by ICP-AES

| Catalysts | $Ni/SiO_2$ | $Ni_3Sb/SiO_2$ | $NiSb/SiO_2$ | $NiSb_3/SiO_2$ |
|---|---|---|---|---|
| Ni mass fraction (wt.%) | 4.770 | 4.916 | 5.006 | 5.941 |
| Sb mass fraction (wt.%) | — | 2.0076 | 5.892 | 12.325 |
| molar ratio (Ni/Sb) | — | 5.080 | 1.763 | 1.000 |

**Table S2** BET surface area and average pore diameter of different catalysts.

| Catalysts | $Ni/SiO_2$ | $Ni_3Sb/SiO_2$ | $NiSb/SiO_2$ | $NiSb_3/SiO_2$ |
|---|---|---|---|---|
| Surface area ($m^2/g$) | 199.8 | 205.1 | 186.3 | 157.5 |
| Average pore diameter (nm) | 28.1 | 25.1 | 28.0 | 26.4 |

**Table S3** Comparison of catalytic performance of different catalysts for the semi-hydrogenation reaction of phenylacetylene.

| Catalysts | T (℃) | Conv. (%) | Sel. (%) | Ref. |
|---|---|---|---|---|
| $NiSb_3/SiO_2$ | 150 | 100 | 95.2 | This Work |
| Ni-rich $AlNi_3$ | 50 | 99 | 88 | 1 |
| $NiZn_3/\alpha$-$Al_2O_3$ | 60 | > 99 | 92 | 2 |
| $Ni_3CuSn/SiO_2$ | 60 | 99.2 | 94.6 | 3 |
| Ni@NC-800 | 110 | 97 | 94 | 4 |
| fcc Ag@hcp Ni | 70 | 100 | 95.1 | 5 |
| $Ni_1$+$Ni_2P_n$@PBNC | 60 | 100 | 96.2 | 6 |
| PdIn-QT | 25 | 96 | 93 | 7 |
| $Pd_1$/Ni@G | 30 | 100 | 93 | 8 |
| $Pd_1Ag_5/g$-$C_3N_4$ | 25 | 98 | > 93 | 9 |
| UiO-67@Pd@UiO-67 | 10 | 100 | 93.1 | 10 |
| $Pd_1$/NC-PHF | 60 | 93.1 | 93.5 | 11 |
| $Pd_1$/ZIF-8 | 120 | 100 | 93.6 | 12 |
| $Pd_{0.5}/Ni_{0.5}$@γ-$Al_2O_3$ | 25 | 98 | 94 | 13 |
| $Pd_6/TiO_2$ | 50 | 94.9 | 94 | 14 |
| $Pd_1$/G | 25 | 100 | 94 | 15 |
| $PPh_3$-Pd/$Al_2O_3$-9 | 25 | 99 | 95 | 16 |
| h–Pd-Mn/NC | 60 | 99 | 95 | 17 |
| Pd-Pb NSs | 40 | 100 | 95.8 | 18 |
| CuPd@ZIF-8 | 25 | 97 | 96 | 19 |
| $Pd_1$@ZSM-5 | 65 | 100 | 95 | 20 |
| $Pd_1$+$Pd_n$@NC/HAP | 30 | 93.8 | 96.1 | 21 |

**Table S4.** Phenylacetylene conversion and styrene selectivity as a function of reaction temperature over $NiSb_3/SiO_2$.

| Catalysts | Temperature (℃) | Time (h) | Conv. (%) | Sel. (%) |
|---|---|---|---|---|
| $NiSb_3/SiO_2$ | 150 | 2 | 100 | 94.4 |
| $NiSb_3/SiO_2$ | 150 | 3 | 100 | 95.8 |
| $NiSb_3/SiO_2$ | 150 | 4 | 100 | 94.9 |

**Table S5.** Hydrogenation of various alkynes over the $NiSb_3/SiO_2$ catalyst.

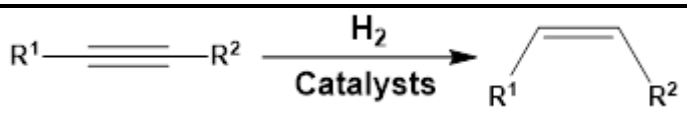


| Entry | Substrates | T (℃) | P (MPa) | Time (h) | Conv. (%) | Sel. (%) |
|---|---|---|---|---|---|---|
| 1 | 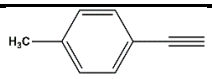 | 140 | 1.0 | 2 | 96.7 | 92.3 |
| 2 | 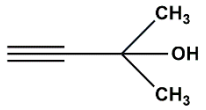 | 80 | 0.5 | 2 | 93.1 | 90.5 |
| 3 | 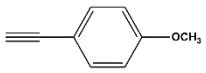 | 110 | 1.0 | 2 | 98.5 | 91.1 |
| 4 | 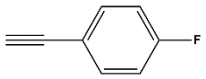 | 100 | 1.0 | 2 | 99.9 | 90.7 |
| 5 | 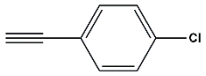 | 100 | 1.0 | 2 | 99.9 | 90.2 |
| 6 | 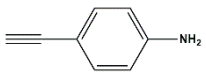 | 110 | 1.0 | 2 | 94.6 | 91.4 |
| 7 | $HC{\equiv}C(CH_2)_3CH_3$ | 150 | 1.0 | 2 | 94.5 | 88.5 |

Reaction conditions: substrate 2 mmol, ethanol 20 mL, catalyst 100 mg.

## References


1 H. Liu, X. Chen, S. Liu, Y. Du, W. Zhu, Z. Hu, M. Armbrüster and C. Liang, *Ind. Eng. Chem. Res.*, 2024, **63**, 3608-3620.

2 Z. Bao, L. Yang, Z. Cheng and Z. Zhou, *Ind. Eng. Chem. Res.*, 2020, **59**, 4322-4332.

3 W. Chen, H. Xu, X. Ma, L. Qi and Z. Zhou, *Chem. Eng. J.*, 2023, **455**, 140565.

4 X. Wang, T. Song, G. Fu and Y. Yang, *ACS Catal.*, 2023, **13**, 11634-11643.

5 J. Su, Y. Ji, S. Geng, L. Li, D. Liu, H. Yu, B. Song, Y. Li, C. W. Pao, Z. Hu, X. Huang, J. Lu and Q. Shao, *Adv. Mater.*, 2024, **36**, 2308839.

6. Z. Chen, Y. Chen, L. Shi, X. Li, G. Xu, X. Zeng, X. Zheng, Z. Qi, K. Zhang, J. Li, S. Zhang, Z. Zhao and Y. Zhang, *Adv. Mater.*, 2024, **36**, 2405733.

7 J. S. Martinez, J. Mazarío, C. W. Lopes, S. Trasobares, J. J. Calvino Gamez, G. Agostini and P. Oña-Burgos, *ACS Catal.*, 2024, **14**, 4768-4785.

8 L. Zhao, X. Qin, X. Zhang, X. Cai, F. Huang, Z. Jia, J. Diao, D. Xiao, Z. Jiang, R. Lu, N. Wang, H. Liu and D. Ma, *Adv. Mater.*, 2022, **34**, 2110455.

9 X. Guo, C. Feng, Z. Yang, S. Hasegawa, K. Motokura and Y. Yang, *ACS Nano*, 2025, **19**, 2788-2798.

10 K. Choe, F. Zheng, H. Wang, Y. Yuan, W. Zhao, G. Xue, X. Qiu, M. Ri, X. Shi, Y. Wang, G. Li and Z. Tang, *Angew. Chem., Int. Ed.*, 2020, **59**, 3650-3657.

11 S. Li, G. Yue, H. Li, J. Liu, L. Hou, N. Wang, C. Cao, Z. Cui and Y. Zhao, *Chem. Eng. J.*, 2023, **454**, 140031.

12 X. Li, F. Zhang, X. Han, J. H. Wang, X. Cui, P. Xing, H. Li and X. M. Zhang, *Nano Res.*, 2023, **16**, 8003-8011.

13 X. Song, F. Shao, Z. Zhao, X. Li, Z. Wei and J. Wang, *ACS Catal.*, 2022, **12**, 14846-14855.

14 J. Tang, K. Jia, R. Zhang, C. Liu, X. Lin, T. Ge, X. Liu, Q. Zhao, W. Liu, D. Ma, H. Fan and J. Huang, *ACS Catal.*, 2024, **14**, 2463-2472.

15 K. Zhang, H. L. Cheng, Y. Wang, Y. Liu, Z. W. Xing, P. Tan, Y. Nian, Y. Han and L. B. Sun, *AIChE J.*, 2025, **71**, e18897.

16 M. Wang, Y. Chen, X. Liu, Z. Zhao, L. Ren, S. Huang, G. Dong, M. Xia, X. Li, Z. Wei and J. Wang, *AIChE J.*, 2024, **70**, e18386.

17 H. Liu, P. Zhu, D. Yang, C. Zhong, J. Li, X. Liang, L. Wang, H. Yin, D. Wang and Y. Li, *J. Am. Chem. Soc.*, 2024, **146**, 2132-2140.

18 C. Shen, Y. Ji, P. Wang, S. Bai, M. Wang, Y. Li, X. Huang and Q. Shao, *ACS Catal.*, 2021, **11**, 5231-5239.

19 L. Li, W. Yang, Q. Yang, Q. Guan, J. Lu, S. H. Yu and H. L. Jiang, *ACS Catal.*, 2020, **10**, 7753-7762.

20 H. Liu, J. Li, X. Liang, H. Ren, H. Yin, L. Wang, D. Yang, D. Wang and Y. Li, *J. Am. Chem. Soc.*, 2024, **146**, 24033-24041.

21 Z. Chen, C. Wang, B. Zhang, J. Li, D. Wang, G. Xu, J. Zhang, M. Peng, D. Ma and Y. Zhang, *Adv. Mater.*, 2025, **37**, 2503841.